


## RESEARCH ARTICLE

# Postmortem quantitative MRI disentangles histological lesion types in multiple sclerosis

Riccardo Galbusera<sup>1,2</sup>  | Erik Bahn<sup>3</sup> | Matthias Weigel<sup>1,2,4</sup> | Sabine Schaedelin<sup>5</sup> | Jonas Franz<sup>3,6,7</sup> | Po-Jui Lu<sup>1,2</sup> | Muhamed Barakovic<sup>1,2</sup> | Lester Melie-Garcia<sup>1,2</sup> | Peter Dechent<sup>8</sup> | Antoine Lutti<sup>9</sup> | Pascal Sati<sup>10</sup> | Daniel S. Reich<sup>11</sup> | Govind Nair<sup>12</sup> | Wolfgang Brück<sup>3</sup> | Ludwig Kappos<sup>2</sup> | Christine Stadelmann<sup>3,13</sup> | Cristina Granziera<sup>1,2</sup>

<sup>1</sup>Translational Imaging in Neurology (ThINK) Basel, Department of Biomedical Engineering, Faculty of Medicine, University Hospital Basel and University of Basel, Basel, Switzerland

<sup>2</sup>Neurologic Clinic and Policlinic, MS Center and Research Center for Clinical Neuroimmunology and Neuroscience Basel (RC2NB), University Hospital Basel and University of Basel, Basel, Switzerland

<sup>3</sup>Institute of Neuropathology, University Medical Center, Göttingen, Germany

<sup>4</sup>Division of Radiological Physics, Department of Radiology, University Hospital Basel, Basel, Switzerland

<sup>5</sup>Clinical Trial Unit, Department of Clinical Research, University Hospital Basel, University of Basel, Basel, Switzerland

<sup>6</sup>Campus Institute for Dynamics of Biological Networks, University of Göttingen, Göttingen, Germany

<sup>7</sup>Max Planck Institute for Experimental Medicine, Göttingen, Germany

<sup>8</sup>Department of Cognitive Neurology, MR-Research in Neurosciences, University Medical Center Göttingen, Göttingen, Germany

<sup>9</sup>Centre for Research in Neuroscience, Department of Clinical Neurosciences, Laboratoire de Recherche en Neuroimagerie (LREN) University Hospital and University of Lausanne, Lausanne, Switzerland

<sup>10</sup>Department of Neurology, Cedars-Sinai Medical Center, Los Angeles, California, USA

<sup>11</sup>Translational Neuroradiology Section, National Institute of Neurological Disorders and Stroke, National Institutes of Health, Bethesda, Maryland, USA

<sup>12</sup>National Institute of Neurological Disorders and Stroke, Bethesda, Maryland, USA

<sup>13</sup>Cluster of Excellence "Multiscale Bioimaging: from Molecular Machines to Network of Excitable Cells (MBExC)", University of Goettingen, Germany

## Correspondence

Cristina Granziera, Translational Imaging in Neurology (ThINK) Basel, Department of Biomedical Engineering, University of Basel Gewerbestrasse 14, 4123 Allschwil, Switzerland. Email: [cristina.granziera@usb.ch](mailto:cristina.granziera@usb.ch)

## Funding information

German Ministry of Education (BMBF; KKNMS German competence network for multiple sclerosis); Swiss National Science Fund, Grant/Award Numbers: PP00P3\_176984, PP00P3\_206151; Ministry of Education; Deutsche Forschungsgemeinschaft; Research Foundation; Deutsche Forschungsgemeinschaft

## Abstract

Quantitative MRI (qMRI) probes the microstructural properties of the central nervous system (CNS) by providing biophysical measures of tissue characteristics. In this work, we aimed to (i) identify qMRI measures that distinguish histological lesion types in postmortem multiple sclerosis (MS) brains, especially the remyelinated ones; and to (ii) investigate the relationship between those measures and quantitative histological markers of myelin, axons, and astrocytes in the same experimental setting. Three fixed MS whole brains were imaged with qMRI at 3T to obtain magnetization transfer ratio (MTR), myelin water fraction (MWF), quantitative T1 (qT1), quantitative susceptibility mapping (QSM), fractional anisotropy (FA) and radial diffusivity (RD) maps. The identification of lesion types (active, inactive, chronic active, or remyelinated) and quantification of tissue components were performed using histological staining methods as well as immunohistochemistry

Riccardo Galbusera and Erik Bahn contributed equally to this study. Christine Stadelmann and Cristina Granziera contributed equally to this study.

This is an open access article under the terms of the [Creative Commons Attribution-NonCommercial](https://creativecommons.org/licenses/by-nc/4.0/) License, which permits use, distribution and reproduction in any medium, provided the original work is properly cited and is not used for commercial purposes.

© 2022 The Authors. *Brain Pathology* published by John Wiley & Sons Ltd on behalf of International Society of Neuropathology.

and immunofluorescence. Pairwise logistic and LASSO regression models were used to identify the best qMRI discriminators of lesion types. The association between qMRI and quantitative histological measures was performed using Spearman's correlations and linear mixed-effect models. We identified a total of 65 lesions. MTR and MWF best predicted the chance of a lesion to be remyelinated, whereas RD and QSM were useful in the discrimination of active lesions. The measurement of microstructural properties through qMRI did not show any difference between chronic active and inactive lesions. MWF and RD were associated with myelin content in both lesions and normal-appearing white matter (NAWM), FA was the measure most associated with axon content in both locations, while MWF was associated with astrocyte immunoreactivity only in lesions. Moreover, we provided evidence of extensive astrogliosis in remyelinated lesions. Our study provides new information on the discriminative power of qMRI in differentiating MS lesions -especially remyelinated ones- as well as on the relative association between multiple qMRI measures and myelin, axon and astrocytes.

#### KEYWORDS

histology, multiple sclerosis, postmortem imaging, quantitative MRI, remyelination

## 1 | INTRODUCTION

Multiple sclerosis (MS) is a chronic, immune-mediated and degenerative disease of the central nervous system, which affects almost three million people worldwide and represents the primary cause of nontraumatic disability in young adults.<sup>1</sup>

Neuropathological investigations have provided important contributions to our understanding of the disease,<sup>2-6</sup> but also to the development of pathologically meaningful imaging biomarkers for inflammation and demyelination.<sup>7-9</sup>

MS lesions are heterogeneous, show a complex cellularity and evolve over time<sup>10</sup>; thus, histologically, a spectrum of focal lesions can be identified<sup>11</sup>: (i) *active*, that is, lesions containing numerous immune cells (monocyte-derived macrophages and phagocytic microglia); (ii) *chronic active (or mixed active/inactive or smoldering lesions)*, that is, lesions showing a rim of activated microglia/macrophages at the lesion edge and loss of myelin/axons in the center; and (iii) *inactive*, that is, hypocellular and demyelinated. In addition, *remyelinated lesions* can be identified histologically and are characterized by shorter and thinner myelin sheaths replacing the destroyed myelin.<sup>12,13</sup> The regenerative process often involves only part of the lesion, mostly at its border, but sometimes it leads to a complete remyelination and thus to the formation of the so-called 'shadow plaques'.<sup>14</sup>

To date, only some of the above-mentioned histological lesion types have been firmly associated to qualitative magnetic resonance imaging (MRI) biomarkers. Indeed, active lesions with significant blood-brain barrier disruption can be identified through gadolinium-enhancement in T1-weighted images, and at least a fraction of chronic active lesions show a rim of increased susceptibility that can be detected with

susceptibility-weighted imaging,<sup>15</sup> phase imaging<sup>9</sup> or quantitative susceptibility mapping (QSM).<sup>16,17</sup> On the other hand, there are no specific imaging correlates for inactive and remyelinated lesions, since the absence of inflammatory activity as measured with gadolinium-enhancement or paramagnetic rim lesions (PRL) does not necessarily identify a lesion as inactive or remyelinated. Previous studies have already evidenced the potential role of (semi)quantitative MRI (i.e., MTR) in discriminating remyelinated lesions.<sup>18-20</sup>

Hence, the goal of this work was to identify quantitative MRI measures that disentangle the histopathological complexity of the MS focal pathology in postmortem human brains, and especially help identifying remyelinated lesions.

Quantitative MRI (qMRI) techniques such as quantitative T1 (qT1), myelin water imaging (MWI), magnetization transfer (MT), and diffusion imaging provide measures that are associated to axon and myelin integrity, iron content, and cellularity in the CNS.<sup>21</sup> Nonetheless, all these metrics are sensitive to more than one tissue component and their relative relationship to specific tissue components (i.e., myelin, axons, cells) has not been comprehensively elucidated in the same experimental setting. Indeed, although studies have been performed to compare some quantitative measures, those are difficult to compare to each other due to the diversity of experimental conditions.<sup>22,23</sup>

In this study, our objectives were: (i) to identify the pattern of qMRI measures that would allow to differentiate histological lesion types in postmortem brains of MS patients and (ii) to investigate the relationship between those qMRI measures and quantitative histological measures of myelin, axons, and astrocytes in the same experimental setting.

## 2 | METHODS

### 2.1 | Specimen preparation and experimental setup

This study was approved by the ethical review committee of the University Medical Center Göttingen. Three whole brains from one female and two male MS patients were provided by the German MS Brain Bank of the Competence Network Multiple Sclerosis (KKNMS). These brains were the same used in our previous study by Rahmzadeh et al.<sup>24</sup> The ages of the patients were 51, 58, and 66 years. The autopsies were performed 24 h post-mortem at the latest and the brains transferred directly to 4% neutral buffered formaldehyde solution. One patient had secondary progressive MS and two suffered from relapsing–remitting MS. Documents on the clinical course of each patient were obtained from the respective attending neurologist and the family doctor (Table 1).

MRI of the whole brains was performed 3–12 months after death. Approximately 1 week prior to scanning, the brains were placed into a custom-built and MRI-compatible container<sup>25–27</sup> and immersed in Fomblin<sup>®</sup> perfluoropolyether (Solvay Specialty Polymers USA, LLC, West Deptford, NJ, USA), a liquid-phase proton-free fluorocarbon which lacks any signal in hydrogen-based MRI.<sup>28</sup> Since air bubbles produce relevant susceptibility artifacts, the bubbles were removed before imaging by suction using a vacuum pump. After this multi-step preparation process, the whole brains were imaged on a clinical 3T whole-body MR system (Magnetom Prisma, Siemens Healthineers, Erlangen, Germany). We employed the built-in body coil for radio-frequency (RF) transmission; for RF reception we used the standard 20-channel phased-array head and neck coil supplied by the manufacturer.

### 2.2 | Ex vivo MRI protocol and image processing

Brain images were acquired with the following sequences, adapted to ex vivo conditions and capabilities, since due to natural tissue decomposition but also to chemical fixation the postmortem tissue's MRI properties are to a certain extent different from those found in vivo<sup>29,30</sup>:

(i) MP2RAGE (670  $\mu\text{m}$  isotropic, TR = 5 s, TE = 1.78 ms, T11 = 194 ms, and T12 = 2500 ms) to obtain quantitative T1 maps (qT1)<sup>31,32</sup>; (ii) Fast Acquisition with Spiral Trajectory and adiabatic T2prep (FAST-T2) (1000  $\mu\text{m}$  isotropic, spiral TR/TE = 9.3 ms/0.94 ms, six T2prep times of [0, 7.5, 17.5, 67.5, 147.5, 307.5] ms) to assess myelin water fraction (MWF), using the cut-off of 20 ms to separate the short and the long T2 components, as suggested by Nguyen et al.<sup>33</sup>; (iii) segmented 3D-EPI (330  $\mu\text{m}$  isotropic, TR = 65 ms, TE = 35 ms, ETL = 13, bandwidth 394 Hz/Pixel) to enable QSM<sup>34</sup>; (iv) proton density weighted (TR = 25 ms, flip angle 5°), and MT prepared (TR = 25 ms, flip angle 5°) RF-spoiled 3D-GRE of identical geometry (570  $\mu\text{m}$  isotropic) to allow MTR map calculation<sup>35</sup>; (v) diffusion tensor imaging: Brain 1: resolution 1.4 mm isotropic, b-value = 0/1400/2000/4000 s/mm<sup>2</sup>: TE = 93.0 ms;  $\delta$  = 28.9 ms;  $\Delta$  = 42.9 ms; Brain 2: resolution 1.5 mm isotropic, b-value = 0/1650/2350/4650 s/mm<sup>2</sup>, TE = 99.0 ms,  $\delta$  = 31.9 ms,  $\Delta$  = 45.9 ms; Brain 3: resolution 1.3 mm isotropic, b-value 0/1350/2650/4000 s/mm<sup>2</sup>, TE = 80.0 ms;  $\delta$  = 22.3 ms;  $\Delta$  = 36.3 ms. Diffusion images were denoised<sup>36</sup> and fractional anisotropy (FA) and radial diffusivity (RD) maps were computed (Figure S1).

### 2.3 | Individualized cutting box and sectioning

In order to ease the registration of the MRI to the histology slices, we designed and 3D-printed an individualized cutting box based on the MRI for each brain, as reported in references [25,26] (Figure 1).

Brain slices were then photographed and the 3D echo planar imaging (3D EPI) images manually registered to the photographs by means of ITK-SNAP.<sup>37</sup>

After the cutting process, we analyzed the slab-matched 3D EPI images to identify potential regions of interest (focal abnormalities in the white matter), which were then dissected and analyzed histologically (Figure S2).

### 2.4 | Histopathological analysis

Tissue blocks were embedded in paraffin and slices of 4  $\mu\text{m}$  thickness were stained for myelin (Luxol Fast Blue/Periodic-Acid Schiff (LFB/PAS)), for axons (Bielschowsky silver impregnation), for iron (DAB-enhanced Turnbull staining), as well as using hematoxylin/eosin (H&E).

Immunohistochemical staining was performed using an avidin–biotin technique. Primary antibodies comprised anti–myelin basic protein (anti-MBP; Dako, Glostrup, Denmark for myelin) and anti-CR3/43 (human HLA-DP, clone CR3/43, for MHC-II expressing microglia/macrophages). After incubation with the primary antibody (applied at the dilutions indicated by the supplier and incubated overnight at 4°C), antibody binding

TABLE 1 Patients' characteristics

Patient	Age	Sex	Disease course	Disease duration	EDSS
1	51	F	RRMS	8 years	4
2	58	M	SPMS	23 years	8
3	66	M	RRMS	17 years	2,5

Abbreviations: EDSS, Expanded Disability Status Scale; F, female; M, male; RRMS, relapsing–remitting MS; SPMS, secondary progressive MS.

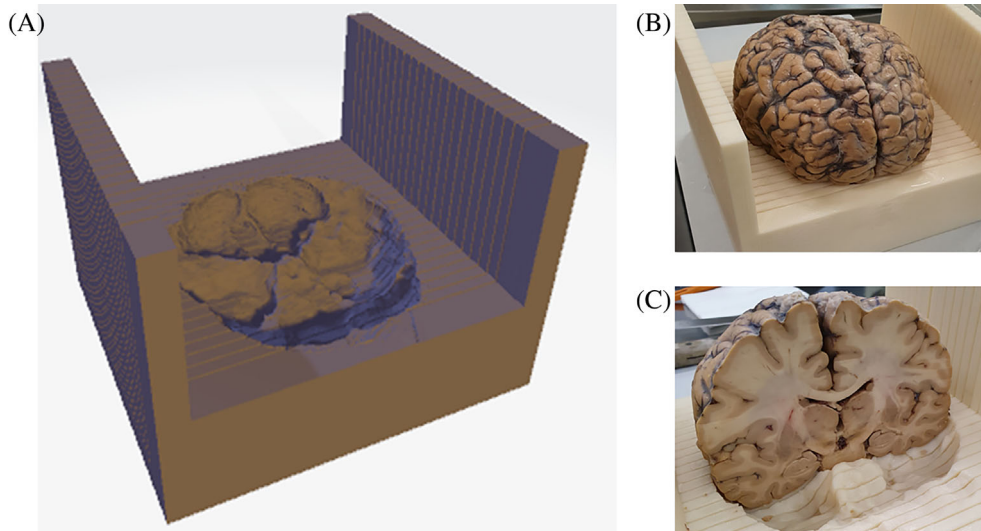


**FIGURE 1** Three-dimensional (3D) model of an individualized cutting box (A), 3D print of the same model (B) and intermediate stage of the cutting process (C).

was visualized using biotinylated secondary antibodies, peroxidase-conjugated avidin, and DAB (Sigma-Aldrich). Double-labeling immunohistochemistry was performed combining DAB and Fast Blue using an alkaline phosphatase-conjugated secondary antibody (Dako, 1:50). Hematoxylin was used as nuclear counterstain. Double immunofluorescence immunohistochemistry was performed using primary antibodies directed against myelin basic protein and neurofilament proteins (cocktail of anti-NF200 [Sigma Aldrich, Missouri, USA], SMI31, SMI32, and SMI311 (Sternberger monoclonals incorporated, Maryland, USA) or astrocytes (cocktail of antibodies against glial fibrillary acidic protein; SYSY, Göttingen, Germany, and Aldh1l1 (aldehyde dehydrogenase 1 family member L1, Merck, Darmstadt, Germany)). Alexa FluorVR488 (Jackson ImmunoResearch Laboratories, Inc.) or CyTM3 (ImmunoResearch Laboratories, Inc.) coupled anti-mouse and anti-rabbit Ig antibodies were used as secondary antibodies. DAPI (4',6-diamidino-2-phenylindol) staining was used for cell nuclei staining.

After histology/IHC, the sections were scanned automatically by a computer-directed microscope stage (Olympus VS120 Soft Imaging Solutions) with a 20 $\times$  objective magnification for further investigations. Digital processing of slide images was performed using an open microscopy OMERO server (version 5.6.3).

## 2.5 | Staging of MS lesions

Lesion staging was performed using LFB/PAS staining and immunohistochemistry for myelin (MBP and BCAS1) and activated microglia/macrophages (human HLA-DP, clone CR3/43), was based on the recent classification system according to Kuhlmann et al.<sup>11</sup> and included the category of lesion with extensive remyelination (shadow plaques), which were defined as proposed

by Patrikios et al. (presence of remyelination in >60% of the plaque area).<sup>12</sup>

Histological image analysis was carried out by identifying the respective regions of interest (ROI) manually, that is, white matter lesions and NAWM. NAWM areas were defined as white matter without or with only sparse microglia activation and, if possible, a minimum distance of 0.5 cm from white matter or cortical lesions.

Lesions were classified into four different groups (active, chronic active, inactive, and remyelinated) based on the detection of focal areas of demyelination/remyelination as well as the presence, density and localization of activated microglia/macrophage and ongoing demyelinating activity. Remyelination was characterized in LFB/PAS staining and MBP and/or BCAS1 immunohistochemistry by subtle myelin pallor when compared to the surrounding NAWM, and absence of macrophages with early myelin degradation products. As mentioned above, we included in the category of remyelinated lesions only lesions with areas of remyelination covering at least 60% of their surface.<sup>12</sup> Myelin regeneration can be found in inactive, chronic active or active lesion types; in case of classification as “remyelinated,” these lesions were excluded from the other three categories in our analysis.

All lesions were assessed and classified by two board-certified neuropathologists (EB, CS).

## 2.6 | MRI-histopathology analysis

We automatically registered all the images to the slab-matched 3D EPI images through Elastix<sup>38,39</sup> using an affine transformation.

White matter lesions (WML) accurately selected on histology and areas of NAWM in their vicinity were easily identified on the corresponding 3D EPI images and manually segmented, on two dimensions, on the same



spatial plane as the histology section, by using ITK-SNAP 3.6.0<sup>37</sup> (Figure S3). The segmentation mask was thereafter checked for quality and consistency on 3D fluid-attenuated inversion recovery (FLAIR) images. All six qMRI scans were registered to the 3D EPI, average intensity values were then computed for each region of interest. We considered the full lesion surface without distinguishing lesion core from lesion edge.

## 2.7 | Quantitative histology

We performed the correlation of MRI data with quantitative histology in a randomly selected subset of lesions and in their corresponding NAWM regions (see also the result section).

Quantification of histochemical (LFB), immunohistochemical (anti-MBP) and immunofluorescence (anti-MBP-, anti-NF- and anti-astrocyte cocktail) staining was performed using in-house methods (JF, RG). Specifically, to analyze MBP, color deconvolution (scikit-image, v0.18.1) of the DAB signal was performed applying the same deconvolution matrix to all images using scikit's predefined RGB to HED deconvolution matrix. LFB color separation was performed by creating an individual color separation matrix for each image manually. The stain separation matrix was defined by annotating the LFB blue stain vector and the hematoxylin blue stain vector for each image. The third vector was defined as the orthogonal vector of the first two. For each ROI, we extracted the mean intensity of color-deconvoluted or immunofluorescence images.

## 2.8 | Statistical analysis

We tested two main H0 hypotheses: (H0-1) qMRI measures sensitive to myelin, axons, cells and tissue structure/anisotropy cannot differentiate histologically defined lesion types and (H0-2) measures derived from qMRI do not relate to myelin, axon, and cell content as measured histologically. For both hypotheses, each qMRI measure was considered independent from the others because they were partially correlated (i.e., we performed a single-model analysis for each qMRI parameter).

To confute H0-1, we performed pairwise logistic regression model using MRI measures as independent variables and histopathological lesion types as dependent variables. We used (i) the Akaike's Information Criterion (AIC) to assess the quality of the model fit (the lower the value, the better the data fit the model); and (ii) the c-statistics to assess the agreement between an observed response and a predictor. A c-value of 1 indicates perfect agreement between predicted and observed response. The results were then confirmed assessing all MRI markers together in a LASSO regression model.

In order to visualize the discriminative capabilities of qMRI regarding histological lesion types, we used a *t*-distributed stochastic neighbor embedding - t-SNE plot-, a statistical algorithm which embeds high dimensional data into lower dimensional data enabling their visualization.

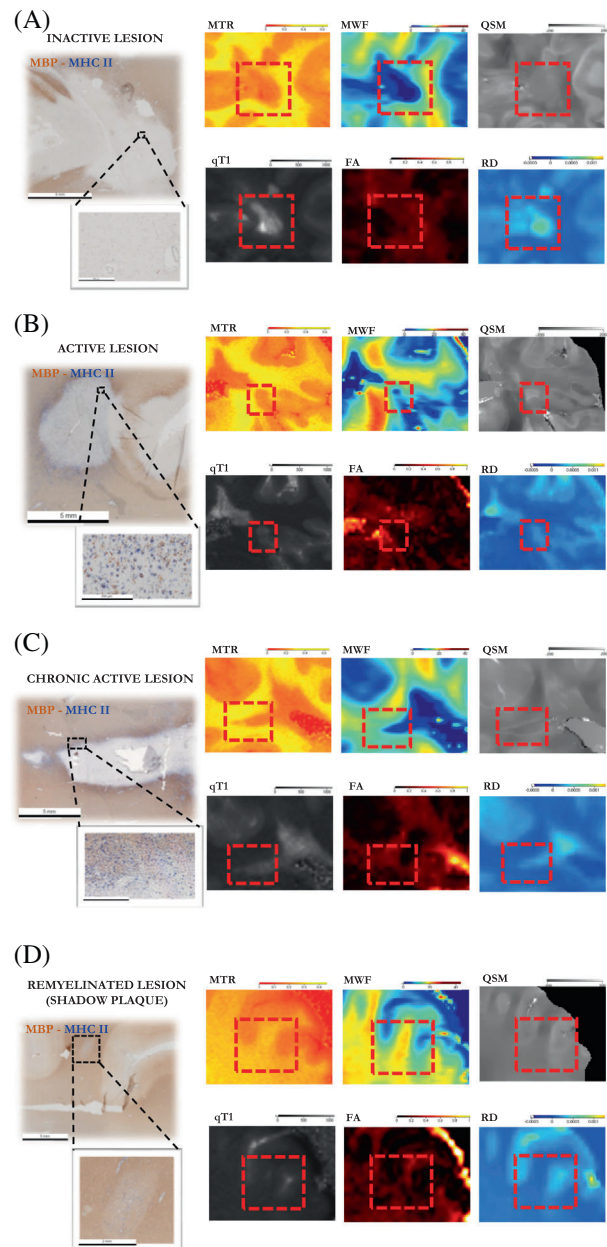


**FIGURE 2** Examples of histopathological lesion types and their correspondent quantitative MRI (qMRI) (MTR, magnetization transfer ratio; MWF, myelin water fraction; QSM, quantitative susceptibility mapping; qT1, quantitative T1; FA, fractional anisotropy; RD, radial diffusivity). (A) Inactive lesion, not showing presence of inflammatory cells; (B) Active lesion, containing numerous microglia/macrophages also in the center; (C) Chronic active lesion, showing presence of activated microglia/macrophages at the edge; (D) Remyelinated lesion (shadow plaque), showing uniformly pale myelin stain across the whole lesion area.

**TABLE 2** Pairwise logistic regression models (without brain as covariate). Each line presents the main results of a separate model.

qMRI	Comparisons	Coef	se	OR	<i>p</i>	c	AIC	N
MTR	Remyelinated vs. chronic active/inactive/active	0.45	0.14	1.57	<0.01	0.83	40.45	65
MWF	Remyelinated vs. chronic active/inactive/active	0.24	0.08	1.27	<0.01	0.78	43.82	65
qT1	Remyelinated vs. chronic active/inactive/active	-0.02	0.01	0.98	<0.01	0.83	43.22	65
QSM	Remyelinated vs. chronic active/inactive/active	-0.03	0.02	0.97	0.0449	0.75	51.28	65
FA	Remyelinated vs. chronic active/inactive/active	-0.81	5.62	0.45	0.8858	0.48	56.26	65
RD	Remyelinated vs. chronic active/inactive/active	-27.91	9.33	0.00	<0.01	0.83	42.54	65
MTR	Inactive vs. chronic active	0.01	0.13	1.01	0.9311	0.49	57.39	47
MWF	Inactive vs. chronic active	-0.01	0.08	0.99	0.9039	0.49	57.39	47
qT1	Inactive vs. chronic active	0.00	0.00	1.00	0.4278	0.58	56.78	47
QSM	Inactive vs. chronic active	0.00	0.01	1.00	0.7462	0.57	57.30	47
FA	Inactive vs. chronic active	1.62	4.73	5.05	0.7320	0.51	57.29	47
RD	Inactive vs. chronic active	1.80	6.02	6.06	0.7646	0.54	57.31	47
MTR	Active vs. remyelinated/chronic active/inactive	0.09	0.10	1.10	0.3540	0.64	55.45	65
MWF	Active vs. remyelinated/chronic active/inactive	0.00	0.07	1.00	0.9725	0.45	56.28	65
qT1	Active vs. remyelinated/chronic active/inactive	-0.01	0.01	0.99	0.0216	0.79	48.08	65
QSM	Active vs. remyelinated/chronic active/inactive	0.03	0.01	1.03	0.0212	0.75	50.47	65
FA	Active vs. remyelinated/chronic active/inactive	-10.78	7.19	0.00	0.1341	0.65	53.55	65
RD	Active vs. remyelinated/chronic active/inactive	-18.68	7.63	0.00	0.0144	0.81	48.53	65

Abbreviations: AIC, Akaike's information criterion; c, c-statistics; Coef, coefficient; FA, fractional anisotropy; MTR, magnetization transfer ratio; MWF, myelin water fraction; N, number of samples; OR, odds ratio; QSM, quantitative susceptibility mapping; qT1, quantitative T1; RD, radial diffusivity.

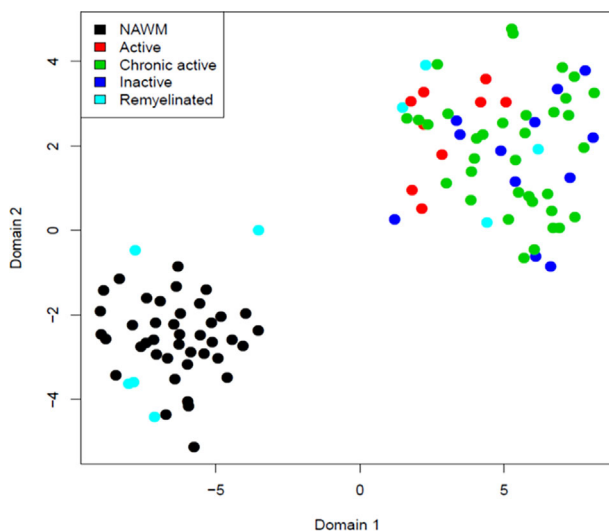


**FIGURE 3** T-distributed stochastic neighbor embedding—t-SNE plot. Remyelinated lesions show different degree of damage and some of them resemble normal-appearing white matter (NAWM). On the other hand, chronic active and inactive lesions are not separable from each other. Active lesions appear to be in between chronic active/inactive lesions and NAWM.

To confute H0-2, we first used Spearman's rank-order correlation between the data obtained from quantitative histology (quantification of myelin, axon, and astrocyte content in selected ROI, see also the paragraph quantitative histology) and the corresponding qMRI measures (i.e., the average of the signal intensity of the corresponding ROI on each MRI sequence).

We further investigated the association between tissue components and MRI through linear mixed-effect models with brains as random effect, to consider the possible lack of independency of lesions belonging to the same brain. In a first model, we assessed whether the association between qMRI and histological measure differs according to the sampling location (lesion vs. NAWM). The second model estimates the association between the MRI and histological measure in lesions and indicates if this association differs in the NAWM.

Statistical analyses were performed in R (version 3.6.3),  $\alpha$  was set at 0.05, two-tailed.

### 3 | RESULTS

We identified on MRI and characterized histologically a total of 65 lesions in three brains: 12 inactive, 35 chronic active, 9 active and 9 (extensively) remyelinated lesions (Figure 2).

Active lesions—a lesion type that is uncommon in brain autopsies—were found in only one brain. The other lesion categories were instead represented in all the brains.

#### 3.1 | Association between histological lesion type and qMRI measures

An overview of the behavior of the quantitative MRI parameters in the different lesion types is given in

**FIGURE 4** Spearman correlation between quantitative MRI metrics and mean myelin basic protein (MBP) (immunohistochemistry, IHC) and Luxol Fast Blue (LFB). Legend dots colors: Black = normal-appearing white matter (NAWM); red = active; green = chronic active; blue = inactive; light blue = remyelinated.

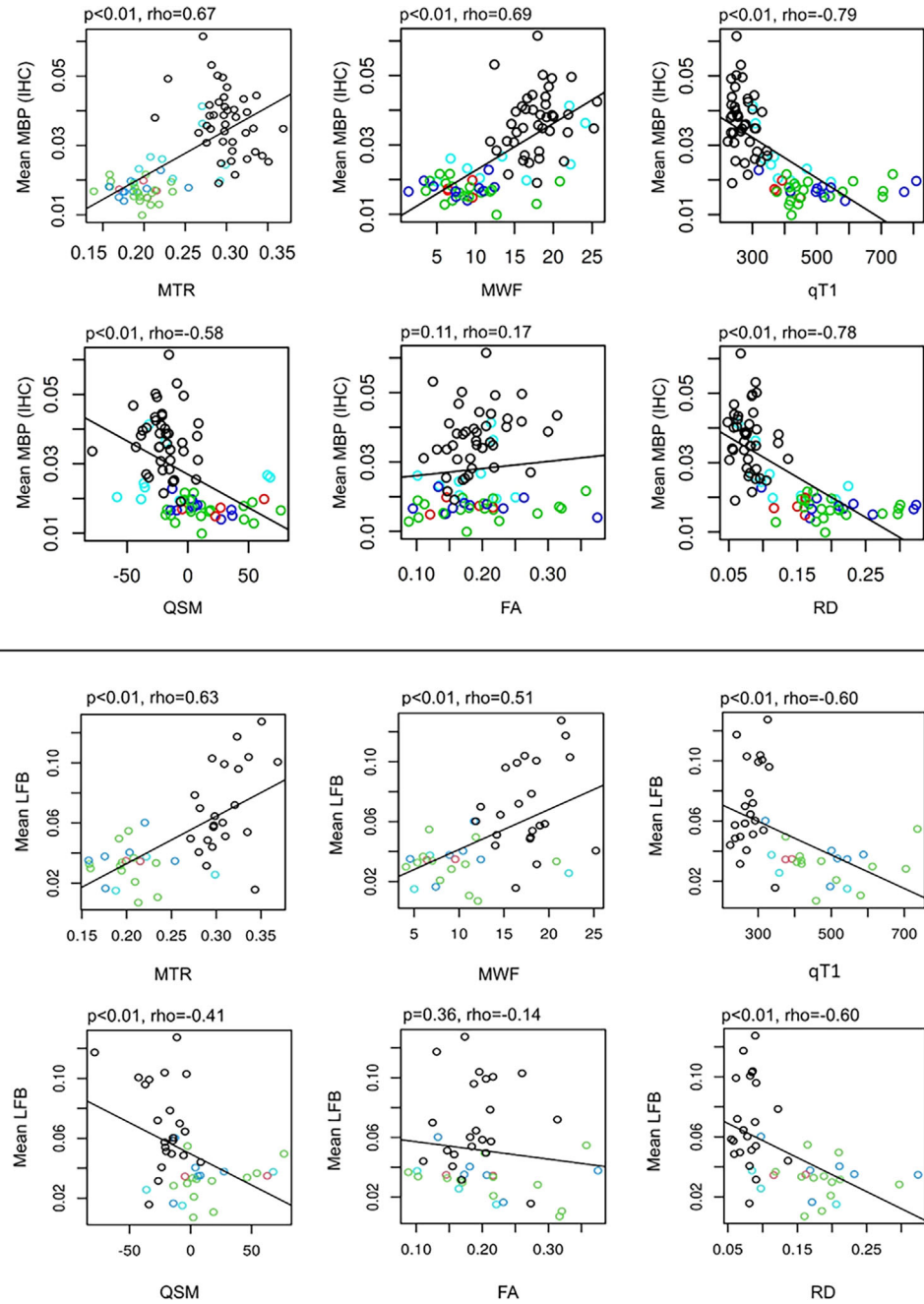


Figure S4. Pairwise logistic regression showed that MTR, RD, qT1, and MWF differentiated between (i) extensive remyelinated and (ii) active, chronic active, and inactive lesions in this order (MTR: AIC = 40.45,  $c = 0.83$ ,  $p < 0.01$ , RD: AIC = 42.54,  $c = 0.83$ ,  $p < 0.01$ , qT1: AIC = 43.22,  $c = 0.83$ ,  $p < 0.01$ , MWF: AIC 43.82,  $c = 0.78$ ,  $p < 0.01$ ). (Table 2) In the LASSO model, MTR and MWF were the strongest predictors of being a remyelinated lesions.

To distinguish active lesions from all other lesion types, qT1, RD, and QSM proved to be the discriminating metrics (qT1: AIC = 48.08,  $c = 0.79$ ,  $p < 0.05$ ; RD: AIC = 48.53,  $c = 0.81$ ,  $p < 0.05$ ; QSM: AIC = 50.47,

$c = 0.75$ ,  $p < 0.05$ ) (Table 2). However, when assessing all MRI markers in a LASSO regression model, the influence of qT1 disappeared.

On the other hand, both the model fit and the concordance seemed to be poor for the separation of inactive from chronic active lesions (Table 2).

When experimental conditions were considered (i.e. inclusion of the brain as random effect in the model), obtained results were very similar for all models with the exception of the model differentiating active lesions from other lesions, where also MTR and MWF appeared discriminative and QSM not anymore.



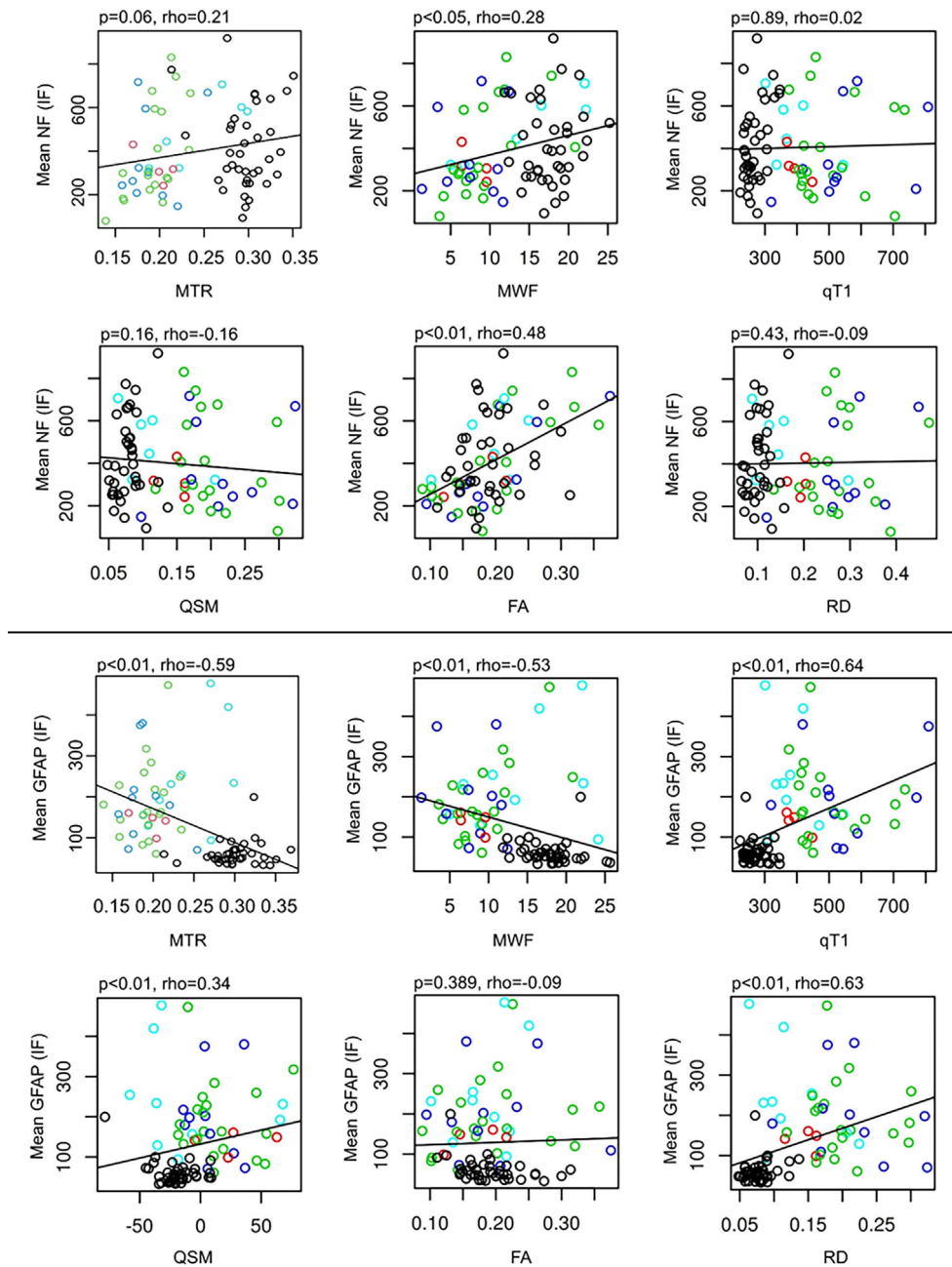


**FIGURE 5** Spearman correlation between quantitative MRI metrics and mean neurofilament cocktail (NF) immunofluorescence (IF) and mean GFAP cocktail immunofluorescence (IF). Legend dots colors: Black = normal-appearing white matter (NAWM); red = active; green = chronic active; blue = inactive; light blue = remyelinated.

A visualization of the discriminative capabilities of qMRI regarding histological lesion types was performed using a t-SNE-plot in Figure 3.

### 3.2 | Correlation of MRI measures with quantitative histology

For the correlation of MRI parameters with quantitative histology we randomly selected a subset of  $n = 43$  lesions (9 extensively-remyelinated, 10 inactive, 20 chronic-active and 4 active) and the corresponding  $n = 43$  regions of NAWM.

#### 3.2.1 | Myelin content

Correlation analysis showed that qT1 correlated best with myelin content quantified with MBP ( $\rho = -0.79, p < 0.01$ ), followed by RD ( $\rho = -0.78, p < 0.01$ ), MWF ( $\rho = 0.69, p < 0.01$ ), MTR ( $\rho = -0.67, p < 0.01$ ) and QSM ( $\rho = -0.58, p < 0.01$ ) (Figure 4).

On the other hand, linear mixed-effect models showed that MTR, MWF, and RD were all associated with MBP-myelin content in the lesion, but only MWF and RD showed a similar association with MBP-myelin content in both lesions and NAWM (Table S1).



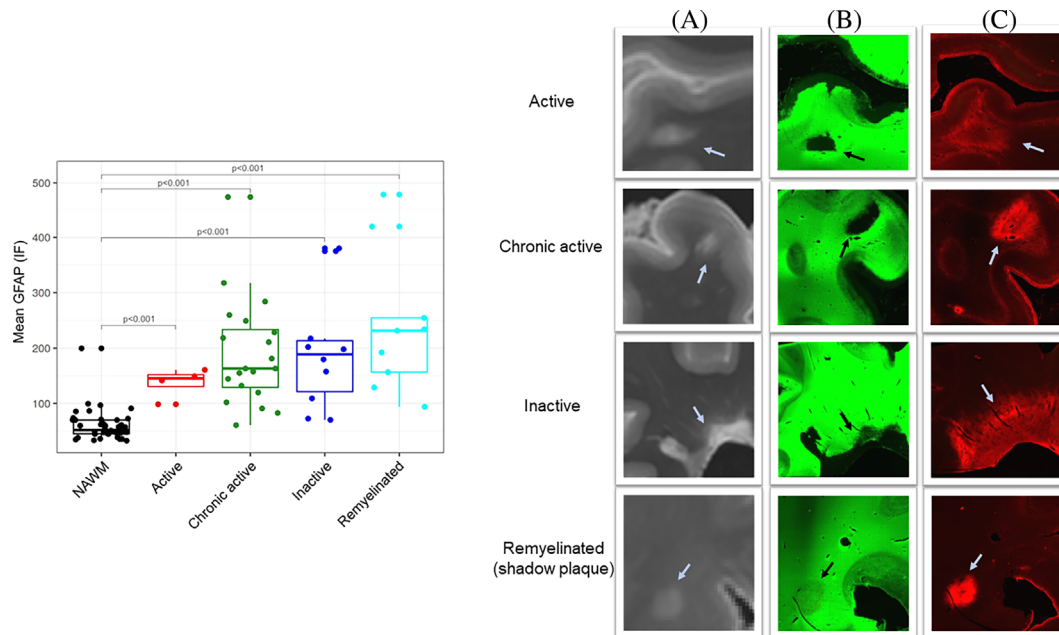


**FIGURE 6** Box plots for astrocyte immunoreactivity, as measured by GFAP immunofluorescence, in the different lesion types. A, MRI fluid-attenuated inversion recovery (FLAIR) image; B, myelin basic protein (MBP) immunofluorescence; C, GFAP immunofluorescence

For the evaluation of myelin content with LFB staining, we could consider 23 lesions (3 remyelinated, 6 inactive, 12 chronic active, 2 active lesions) and 25 NAWM regions. We had to exclude 20 blocks stained with LFB from the analysis because of their not comparable staining intensity for color deconvolution. Again, all MRI parameters but FA correlated with LFB-myelin content (in the order: MTR  $\rho = 0.63$ , qT1  $\rho = -0.60$ , RD  $\rho = -0.60$ , MWF  $\rho = 0.51$ , QSM  $\rho = -0.41$ ;  $p < 0.01$  for all parameters) (Figure 4). However, linear mixed-effect models did not show any significant association between MRI and LFB myelin content (Table S2).

### 3.2.2 | Axonal content

Regarding the analysis of axonal content by means of immunofluorescence for neurofilament (NF), we could include 39 lesions (6 remyelinated, 10 inactive, 19 chronic active, 4 active lesions) versus 39 NAWM regions. FA correlated with neurofilament immunoreactivity ( $\rho = 0.49$ ,  $p < 0.01$ ), followed by MWF ( $\rho = 0.27$ ,  $p < 0.01$ ) (Figure 5). In both linear mixed-effect models, FA and MWF exhibited an association with axonal content, which was similar in lesions and NAWM (Table S3).

### 3.2.3 | Astrocyte immunoreactivity

All qMRI measures except for FA showed moderate to small correlations with astrocyte immunoreactivity (in the order: qT1  $\rho = 0.64$ , RD  $\rho = 0.63$ , MWF

$\rho = -0.53$ , MTR  $\rho = -0.59$ , QSM  $\rho = 0.34$ ;  $p < 0.01$  for all parameters), (Figure 5).

MWF was the only parameter associated with astrocyte immunoreactivity in lesions, and this association was independent from experimental conditions and sampling location (Table S4).

All lesion types (active, chronic active, inactive and extensive-remyelinated) showed astrocyte immunoreactivity in comparison to NAWM areas,  $p < 0.001$  (Figure 6).

## 4 | DISCUSSION

The identification of surrogate markers for remyelination represents one major unmet need for both the development of remyelinating and restorative therapies in MS patients, and for the stratification of patients that might most benefit of reparative strategies.

In this work, we have studied six qMRI measures that theoretically exhibit differential sensitivity and specificity to myelin, axon, and cells characteristics.<sup>21</sup>

Our data show that MWF and MTR best predict a lesion to be extensively-remyelinated, whereas MWF, MTR and also qT1 could differentiate these lesions from all the other histological types. However, the small sample size should be noted as a limitation of this study. QSM did not show high discriminative value for remyelinated lesions in the present study probably because, here, we pooled together fully remyelinated and active, presumably still remyelinating lesions in one group, whereas in the work of Rahmzadeh R. et al.,<sup>24</sup> we distinguished fully remyelinated and probably actively remyelinating

lesions based on their qualitative appearance in QSM (i.e. fully remyelinated lesions appeared there hypo/isointense in QSM, whereas putative actively remyelinating lesions appeared hyperintense).

To date, there is no gold standard imaging biomarker for remyelinated lesions.<sup>40</sup> Different approaches have been proposed so far based on the longitudinal changes of myelin-sensitive measures such as MTR, MWF, RD, qT1, which have been employed in phase II clinical trials with disappointing results.<sup>41</sup> Very recently, qT1 at 7 T MRI was proposed to track lesional myelination changes over time in vivo in MS patients.<sup>42</sup> Yet, while some of these studies provided correlation analyses between qMRI measures and myelin content in lesions,<sup>40–42</sup> none of them assessed the discriminative power of qMRI measures for remyelinated lesions.

Our results confirm previous findings by showing that MTR, MWF, and qT1 are capable to differentiate remyelinated lesions from the others, but also extend existing knowledge by supporting first evidence of the superior discriminative capability of MTR and MWF for extensively remyelinated lesions. These data therefore pave the path to imaging strategies for assessing the presence of remyelinated lesions in clinical studies and in clinical practice.

As to chronic active lesions, from a qualitative perspective they may be identified using susceptibility-based MRI, which captures their characteristic rim of activated iron-laden microglia/macrophages (paramagnetic rim lesions, PRL).<sup>9,15–17</sup> PRL were shown to exhibit a more destructive nature than lesions without a rim (encompassing other chronic lesions but also remyelinated lesions),<sup>33</sup> as well as a tendency to slowly grow over time.<sup>43</sup> Interestingly, our data provided new evidence that chronic active (PRL) and chronic inactive lesions have a similar extent of qMRI alterations, suggesting that these two lesion types share a similar level of tissue destruction, although the first lesion type has shown a dynamic towards expansion of damage and the latter not.

Concerning the identification of active lesions, RD and QSM proved to be the strongest discriminative measures. Also, our results suggested that active lesions exhibit less microstructural damage than chronic active and inactive lesions, but more than the damage observed in extensively-remyelinated lesions. These data confirm and extend previous knowledge that active lesions may either efficiently repair or face further damage and progress to a chronic active and/or to an inactive lesion.<sup>44</sup>

Although all previously mentioned qMRI measures exhibit some sensitivity to myelin, none of them is myelin-specific.<sup>21</sup> In fact, the MT contrast is also sensitive to macromolecules found in the axonal and cellular membranes and MTR exhibits a certain degree of T1 sensitivity that further decreases its specificity to myelin.<sup>44</sup> MWF is thought to be more specific than the MT-based contrast for assessing myelin characteristics<sup>45</sup>; however, it has been also shown that acquisition schemes for MWF,

and in particular the one based on Carr–Purcell–Meiboom–Gill (CPMG) and Gradient And Spin Echo, are sensitive to iron accumulation.<sup>46</sup> The one applied in this study, FAST-T2,<sup>33</sup> is theoretically insensitive to iron presence due to the short T2 that is achieved using a spiral acquisition scheme. Nevertheless, since a cut-off of 20 ms is applied to define the pool of myelin-water, it could be that some non-myelin water is also included in the myelin pool. On the other hand, RD—a DTI parameter that was related to myelin content in animal models of MS and in the human MS spinal cord<sup>47–49</sup>—suffers from low specificity in areas of crossing fibers and low signal to noise.<sup>50</sup> Last, qT1 has been shown to correlate with both myelin and axon content in the CNS, but also with iron and cell accumulation.<sup>42,51</sup>

Numerous studies assessed the relationship between each of the above-mentioned qMRI measures and myelin content in the CNS tissue<sup>22,23,53</sup>; nevertheless, all these studies have been performed in different experimental conditions, so that their results are difficult to compare. To date, only few previous work compared the relationship of multiple qMRI measures with myelin content,<sup>22,23,53</sup> mostly in spinal cord tissue<sup>52</sup> and brain slices.<sup>19,30</sup> Besides, results obtained in those studies are sometimes contradictory<sup>23</sup>: for example, qT1 and qT2 were reported to show low correlation values with myelin content in some studies<sup>54</sup> and very high in others.<sup>30</sup> Also the reported correlation coefficient between MTR and myelin is variable, ranging from 0.36<sup>55</sup> to 0.71.<sup>20</sup>

To overcome these challenges, we planned a correlation analysis between multiple qMRI measures and measures of myelin, axon, and astrocyte content using the same experimental conditions.

Our data show that all qMRI measures but FA exhibited moderate to high correlation with myelin content ( $r = 0.58–0.79$ ), although only MWF and RD were associated to myelin content in both lesions and NAWM, independently of the sample type (i.e., brain). Moreover, MWF and RD were the only measures showing the same association with myelin content in lesions and in the NAWM, hereby confirming previous results obtained with MWF<sup>56</sup> and extending them to RD. The fact that RD exhibits such an independent association with myelin content is quite surprising but also very encouraging, since this measure is easily derived from a clinically compatible MR sequence such as DTI. Nonetheless, as previously mentioned, RD should be used with caution because its relationship with myelin may vary in regions containing crossing fibers.<sup>51</sup>

When myelin content was assessed with a phospholipid-staining (LFB) instead of a protein staining (MBP), we could not observe any significant associations with MRI measures in the linear mixed-effect models. Nevertheless, we have to consider that this analysis was performed in a smaller group of lesions than that on MBP-stained sections.

Regarding axon content, the intensity of NF-immunofluorescence positively correlated with FA and

—to a lesser extent—MWF. While the observed connection of FA with axonal content is in line with previous studies,<sup>56,57</sup> the association of MWF with the amount of axons has not been previously described and may underlie the strong relationship between the presence of axons and myelin in normal appearing tissue and MS lesions.

Last, we did not observe any significant associations between qMRI and astrocyte immunoreactivity, which is in line with some previous observations with single qMRI parameters.<sup>19,30</sup> However, when looking exclusively at the lesion areas, we observed that MWF was positively correlated with the presence of astrocytes, which may be due to a possible association between these cells and the remyelination process (Figure 6). Indeed, we have newly observed an extensive presence of astrocytes in remyelinated lesions: this appears to be in line with recent studies indicating that astrocytes are key regulators for the removal of damaged myelin through recruitment of microglia, before remyelination can take place.<sup>58</sup> This finding might also explain why a completely remyelinated lesion still exhibits a T2-hyperintensity in conventional MRI images. Indeed, the accumulation of astrocytes would increase the intracellular water pool with a consequent increase in T2. Moreover, also a lower myelin content in those areas could play a role. Whether an increase in myelin water in remyelinated axons might contribute to the hyperintense signal in these lesions is however still unclear. In future studies, we will investigate more in detail the cellular composition of the remyelinated lesions and evaluate if there is any relationship between the astrocyte content and the presence of microglia. To note is also that both inactive and chronic active lesions showed a high astrocyte-content that was not related to remyelinating activity, confirming hereby recent knowledge.<sup>59,60</sup>

MR-histology studies are complex and require targeted expertise in both postmortem MRI and histopathology to achieve optimal data acquisition and pairing of information obtained from imaging and histological data. In this work, we minimized the challenges of data registration by using the approach proposed by Luciano et al.<sup>26</sup> Secondly, we have scanned the whole brain and not brain specimens or slices, therefore providing a comprehensive view of MS pathology. However, although the obtained sample size was adequate to explore the primary hypotheses, it was in part limited for secondary analyses (i.e., active lesions, LFB). In addition, the histological analysis performed did not allow to assess the presence of myelin structural abnormalities (e.g. swellings, blisters),<sup>62</sup> which might have influenced the applied qMRI measures.

In conclusion, we expanded the evidence that MWF and MTR are useful markers of remyelination. Our results showed that also DTI-derived measures may well serve the purpose of measuring myelin in the brain of MS patients. Moreover, we provided evidence of an extensive astrogliosis in all lesion types, even in remyelinated ones, suggesting a potential role of astrocytes in myelin

regeneration. Future studies should aim at further characterizing astrocyte function in the different lesion types and shed light on their role in lesion initiation and resolution.

## AUTHOR CONTRIBUTIONS

RG, CS, CG contributed to the study concept and design; EB, JF, WB and CS performed histological evaluation; MW fine-tuned the post-mortem MRI protocols. RG, MW, PL, MB, LG, PD collected and analyzed MRI data. SS, RG and CG contributed to statistical analysis; RG and CG wrote the first draft. EB, MW, SS, JF, PL, MB, LM, PD, AL, PS, DR, GN, WB, LK and CS critically reviewed the manuscript.

## FUNDING INFORMATION

This work was funded by the Swiss National Science Fund PP00P3\_176984 and PP00P3\_206151 and supported by the German Ministry of Education (BMBF; KKNMS German competence network for multiple sclerosis). Daniel S. Reich received support from the Intramural Research Program of NINDS. Christine Stadelmann received funding from the Deutsche Forschungsgemeinschaft (DFG, German Research Foundation)—CRC 274/1—Project ID 408885537 B01, the DFG Sta 1389/5–1 (individual research grant) and is supported by the Deutsche Forschungsgemeinschaft under Germany's Excellence Strategy (EXC 2067/1–390729940). Jonas Franz was supported by the clinician scientist program of the CRC 274.

## CONFLICT OF INTEREST

The authors declare that they have no competing interests.

## DATA AVAILABILITY STATEMENT

The datasets generated and analyzed in this study are available from the corresponding author on a reasonable request.

## ETHICS STATEMENT

This study was approved by the ethical review committee of the University Medical Center Göttingen.

## ORCID

Riccardo Galbusera  <https://orcid.org/0000-0002-3092-8737>

## REFERENCES

1. Koch-Henriksen N, Sørensen PS. The changing demographic pattern of multiple sclerosis epidemiology. *Lancet Neurol*. 2010;9(5): 520–32. [https://doi.org/10.1016/S1474-4422\(10\)70064-8](https://doi.org/10.1016/S1474-4422(10)70064-8)
2. Adams CW, Poston RN, Buk SJ. Pathology, histochemistry and immunocytochemistry of lesions in acute multiple sclerosis. *J Neurol Sci*. 1989;92(2–3):291–306. [https://doi.org/10.1016/0022-510x\(89\)90144-5](https://doi.org/10.1016/0022-510x(89)90144-5)
3. Lucchinetti C, Brück W, Parisi J, Scheithauer B, Rodriguez M, Lassmann H. Heterogeneity of multiple sclerosis lesions: implications for the pathogenesis of demyelination. *Ann Neurol*. 2000;

- 47(6):707–17. [https://doi.org/10.1002/1531-8249\(200006\)47:6<707::aid-ana3>3.0.co;2-q](https://doi.org/10.1002/1531-8249(200006)47:6<707::aid-ana3>3.0.co;2-q)
4. Barnett MH, Prineas JW. Relapsing and remitting multiple sclerosis: pathology of the newly forming lesion. *Ann Neurol*. 2004; 55(4):458–68. <https://doi.org/10.1002/ana.20016>
  5. Prineas JW, Kwon EE, Cho ES, Sharer LR, Barnett MH, Oleszak EL, et al. Immunopathology of secondary-progressive multiple sclerosis. *Ann Neurol*. 2001;50(5):646–57. <https://doi.org/10.1002/ana.1255>
  6. Lucchinetti CF, Bruck W, Lassmann H. Evidence for pathogenic heterogeneity in multiple sclerosis. *Ann Neurol*. 2004;56(2):308. <https://doi.org/10.1002/ana.20182>
  7. Brück W, Bitsch A, Kolenda H, Brück Y, Stiefel M, Lassmann H. Inflammatory central nervous system demyelination: correlation of magnetic resonance imaging findings with lesion pathology. *Ann Neurol*. 1997;42(5):783–93. <https://doi.org/10.1002/ana.410420515>
  8. Bouman PM, Steenwijk MD, Pouwels PJW, Schoonheim MM, Barkhof F, Jonkman LE, et al. Histopathology-validated recommendations for cortical lesion imaging in multiple sclerosis. *Brain*. 2020;143(10):2988–97. <https://doi.org/10.1093/brain/awaa233>
  9. Absinta M, Sati P, Masuzzo F, Nair G, Sethi V, Kolb H, et al. Association of chronic active multiple sclerosis lesions with disability in vivo. *JAMA Neurol*. 2019;76(12):1474–83. <https://doi.org/10.1001/jamaneurol.2019.2399>
  10. Stadelmann C, Timmler S, Barrantes-Freer A, Simons M. Myelin in the central nervous system: structure, function, and pathology. *Physiol Rev*. 2019;99(3):1381–431. <https://doi.org/10.1152/physrev.00031.2018>
  11. Kuhlmann T, Ludwin S, Prat A, Antel J, Brück W, Lassmann H. An updated histological classification system for multiple sclerosis lesions. *Acta Neuropathol (Berl)*. 2017;133(1):13–24. <https://doi.org/10.1007/s00401-016-1653-y>
  12. Patrikios P, Stadelmann C, Kutzelnigg A, Rauschka H, Schmidbauer M, Laursen H, et al. Remyelination is extensive in a subset of multiple sclerosis patients. *Brain J Neurol*. 2006; 129(Pt 12):3165–72. <https://doi.org/10.1093/brain/aw1217>
  13. Prineas JW, Connell F. Remyelination in multiple sclerosis. *Ann Neurol*. 1979;5(1):22–31. <https://doi.org/10.1002/ana.410050105>
  14. Goldschmidt T, Antel J, König FB, Brück W, Kuhlmann T. Remyelination capacity of the MS brain decreases with disease chronicity. *Neurology*. 2009;72(22):1914–21. <https://doi.org/10.1212/WNL.0b013e3181a8260a>
  15. Clarke MA, Pareto D, Pessini-Ferreira L, Arrambide G, Alberich M, Crescenzo F, et al. Value of 3T susceptibility-weighted imaging in the diagnosis of multiple sclerosis. *AJNR Am J Neuroradiol*. 2020;41(6):1001–8. <https://doi.org/10.3174/ajnr.A6547>
  16. Maggi P, Sati P, Nair G, Cortese ICM, Jacobson S, Smith BR, et al. Paramagnetic rim lesions are specific to multiple sclerosis: an international multicenter 3T MRI study. *Ann Neurol*. 2020;88(5): 1034–42. <https://doi.org/10.1002/ana.25877>
  17. Gillen KM, Mubarak M, Park C, Ponath G, Zhang S, Dimov A, et al. QSM is an imaging biomarker for chronic glial activation in multiple sclerosis lesions. *Ann Clin Transl Neurol*. 2021;8(4): 877–86. <https://doi.org/10.1002/acn3.51338>
  18. Barkhof F, Bruck W, De Groot CJA, et al. Remyelinated lesions in multiple sclerosis: magnetic resonance image appearance. *Arch Neurol*. 2003;60(8):1073–81. <https://doi.org/10.1001/archneur.60.8.1073>
  19. Schmierer K, Scaravilli F, Altmann DR, Barker GJ, Miller DH. Magnetization transfer ratio and myelin in postmortem multiple sclerosis brain. *Ann Neurol*. 2004;56(3):407–15. <https://doi.org/10.1002/ana.20202>
  20. Schmierer K, Tozer DJ, Scaravilli F, Altmann DR, Barker GJ, Tofts PS, et al. Quantitative magnetization transfer imaging in postmortem multiple sclerosis brain. *J Magn Reson Imaging JMRI*. 2007;26(1):41–51. <https://doi.org/10.1002/jmri.20984>
  21. Granziera C, Wuerfel J, Barkhof F, Calabrese M, de Stefano N, Enzinger C, et al. Quantitative magnetic resonance imaging towards clinical application in multiple sclerosis. *Brain J Neurol*. 2021;144(5):1296–311. <https://doi.org/10.1093/brain/awab029>
  22. Mancini M, Karakuzu A, Cohen-Adad J, Cercignani M, Nichols TE, Stikov N. An interactive meta-analysis of MRI biomarkers of myelin. *Elife*. 2020;9:e61523. <https://doi.org/10.7554/eLife.61523>
  23. van der Weijden CWJ, Garcia DV, Borra RJH, Thurner P, Meilof JF, van Laar PJ, et al. Myelin quantification with MRI: a systematic review of accuracy and reproducibility. *Neuroimage*. 2021;226:117561. <https://doi.org/10.1016/j.neuroimage.2020.117561>
  24. Rahmzadeh R, Galbusera R, Lu PJ, Bahn E, Weigel M, Barakovic M, et al. A new advanced MRI biomarker for remyelinated lesions in multiple sclerosis. *Ann Neurol*. 2022;92(3):486–502. <https://doi.org/10.1002/ana.26441>
  25. Absinta M, Nair G, Filippi M, Ray-Chaudhury A, Reyes-Mantilla MI, Pardo CA, et al. Postmortem magnetic resonance imaging to guide the pathologic cut: individualized, 3-dimensionally printed cutting boxes for fixed brains. *J Neuropathol Exp Neurol*. 2014;73(8):780–8. <https://doi.org/10.1097/NEN.000000000000096>
  26. Luciano NJ, Sati P, Nair G, Guy JR, Ha SK, Absinta M, et al. Utilizing 3D printing technology to merge MRI with histology: a protocol for brain sectioning. *J Vis Exp JoVE*. 2016;118. <https://doi.org/10.3791/54780>
  27. Griffin AD, Turtzo LC, Parikh GY, Tolpygo A, Lodato Z, Moses AD, et al. Traumatic microbleeds suggest vascular injury and predict disability in traumatic brain injury. *Brain J Neurol*. 2019;142(11):3550–64. <https://doi.org/10.1093/brain/awz290>
  28. Li R, Liu X, Sidabras JW, Paulson ES, Jesmanowicz A, Nencka AS, et al. Restoring susceptibility induced MRI signal loss in rat brain at 9.4 T: a step towards whole brain functional connectivity imaging. *PLoS One*. 2015;10(4):e0119450. <https://doi.org/10.1371/journal.pone.0119450>
  29. Augustinack JC, van der Kouwe AJW. Postmortem imaging and neuropathologic correlations. *Handb Clin Neurol*. 2016;136: 1321–39. <https://doi.org/10.1016/B978-0-444-53486-6.00069-7>
  30. Schmierer K, Wheeler-Kingshott CA, Tozer DJ, et al. Quantitative magnetic resonance of post mortem multiple sclerosis brain before and after fixation. *Magn Reson Med*. 2008;59(2):268–77. <https://doi.org/10.1002/mrm.21487>
  31. Marques JP, Kober T, Krueger G, van der Zwaag W, Van de Moortele PF, Gruetter R. MP2RAGE, a self bias-field corrected sequence for improved segmentation and T1-mapping at high field. *Neuroimage*. 2010;49(2):1271–81. <https://doi.org/10.1016/j.neuroimage.2009.10.002>
  32. Weigel M, Galbusera R, Rahmzadeh R, Barakovic M, Lu P, Kappos L, et al. Postmortem whole-brain MP2RAGE optimization at 3T: a new imaging window into multiple sclerosis cortical pathology. *ISMRM*. 2020; Poster n. 1759. Accessed May 24, 2021. [https://www.ismrm.org/20/program\\_files/PP01.htm](https://www.ismrm.org/20/program_files/PP01.htm)
  33. Nguyen TD, Deh K, Monohan E, Pandya S, Spincemaille P, Raj A, et al. Feasibility and reproducibility of whole brain myelin water mapping in 4 minutes using fast acquisition with spiral trajectory and adiabatic T2prep (FAST-T2) at 3T. *Magn Reson Med*. 2016;76(2):456–65. <https://doi.org/10.1002/mrm.25877>
  34. Liu T, Xu W, Spincemaille P, Avestimehr AS, Wang Y. Accuracy of the morphology enabled dipole inversion (MEDI) algorithm for quantitative susceptibility mapping in MRI. *IEEE Trans Med Imaging*. 2012;31(3):816–24. <https://doi.org/10.1109/TMI.2011.2182523>
  35. Tabelow K, Balteau E, Ashburner J, Callaghan MF, Draganski B, Helms G, et al. hMRI - a toolbox for quantitative MRI in neuroscience and clinical research. *Neuroimage*. 2019;194:191–210. <https://doi.org/10.1016/j.neuroimage.2019.01.029>
  36. Veraart J, Novikov DS, Christiaens D, Ades-Aron B, Sijbers J, Fieremans E. Denoising of diffusion MRI using random matrix



- theory. *Neuroimage*. 2016;142:394–406. <https://doi.org/10.1016/j.neuroimage.2016.08.016>
37. Yushkevich PA, Piven J, Hazlett HC, Smith RG, Ho S, Gee JC, et al. User-guided 3D active contour segmentation of anatomical structures: significantly improved efficiency and reliability. *Neuroimage*. 2006;31(3):1116–28. <https://doi.org/10.1016/j.neuroimage.2006.01.015>
  38. Klein S, Staring M, Murphy K, Viergever MA, Pluim JPW. Elastix: a toolbox for intensity-based medical image registration. *IEEE Trans Med Imaging*. 2010;29(1):196–205. <https://doi.org/10.1109/TMI.2009.2035616>
  39. Shamonin DP, Bron EE, Lelieveldt BPF, Smits M, Klein S, Staring M, et al. Fast parallel image registration on CPU and GPU for diagnostic classification of Alzheimer's disease. *Front Neuroinform*. 2013;7:50. <https://doi.org/10.3389/fninf.2013.00050>
  40. Wang CT, Barnett M, Barnett Y. Imaging the multiple sclerosis lesion: insights into pathogenesis, progression and repair. *Curr Opin Neurol*. 2019;32(3):338–45. <https://doi.org/10.1097/WCO.0000000000000698>
  41. Oh J, Ontaneda D, Azevedo C, Klawiter EC, Absinta M, Arnold DL, et al. Imaging outcome measures of neuroprotection and repair in MS: a consensus statement from NAIMS. *Neurology*. 2019; 92(11):519–33. <https://doi.org/10.1212/WNL.0000000000007099>
  42. Kolb H, Absinta M, Beck ES, Ha SK, Song Y, Norato G, et al. 7T MRI differentiates remyelinated from demyelinated multiple sclerosis lesions. *Ann Neurol*. 2021;90(4):612–26. <https://doi.org/10.1002/ana.26194>
  43. Dal-Bianco A, Grabner G, Kronnerwetter C, Weber M, Höftberger R, Berger T, et al. Slow expansion of multiple sclerosis iron rim lesions: pathology and 7 T magnetic resonance imaging. *Acta Neuropathol (Berl)*. 2017;133(1):25–42. <https://doi.org/10.1007/s00401-016-1636-z>
  44. Gaitán MI, Shea CD, Evangelou IE, Stone RD, Fenton KM, Bielekova B, et al. Evolution of the blood-brain barrier in newly forming multiple sclerosis lesions. *Ann Neurol*. 2011;70(1):22–9. <https://doi.org/10.1002/ana.22472>
  45. Campbell JSW, Leppert IR, Narayanan S, Boudreau M, Duval T, Cohen-Adad J, et al. Promise and pitfalls of g-ratio estimation with MRI. *Neuroimage*. 2018;182:80–96. <https://doi.org/10.1016/j.neuroimage.2017.08.038>
  46. Laule C, Leung E, Lis DKB, et al. Myelin water imaging in multiple sclerosis: quantitative correlations with histopathology. *Mult Scler Houndmills Basingstoke Engl*. 2006;12(6):747–53. <https://doi.org/10.1177/1352458506070928>
  47. Birkl C, Birkl-Toeglhofer AM, Endmayr V, Höftberger R, Kasprian G, Krebs C, et al. The influence of brain iron on myelin water imaging. *Neuroimage*. 2019;199:545–52. <https://doi.org/10.1016/j.neuroimage.2019.05.042>
  48. Song SK, Sun SW, Ramsbottom MJ, Chang C, Russell J, Cross AH. Dysmyelination revealed through MRI as increased radial (but unchanged axial) diffusion of water. *Neuroimage*. 2002;17(3):1429–36. <https://doi.org/10.1006/nimg.2002.1267>
  49. Janve VA, Zu Z, Yao SY, Li K, Zhang FL, Wilson KJ, et al. The radial diffusivity and magnetization transfer pool size ratio are sensitive markers for demyelination in a rat model of type III multiple sclerosis (MS) lesions. *Neuroimage*. 2013;74:298–305. <https://doi.org/10.1016/j.neuroimage.2013.02.034>
  50. Klawiter EC, Schmidt RE, Trinkaus K, Liang HF, Budde MD, Naismith RT, et al. Radial diffusivity predicts demyelination in ex vivo multiple sclerosis spinal cords. *Neuroimage*. 2011;55(4):1454–60. <https://doi.org/10.1016/j.neuroimage.2011.01.007>
  51. Wheeler-Kingshott CAM, Cercignani M. About “axial” and “radial” diffusivities. *Magn Reson Med*. 2009;61(5):1255–60. <https://doi.org/10.1002/mrm.21965>
  52. Mottershead JP, Schmierer K, Clemence M, et al. High field MRI correlates of myelin content and axonal density in multiple sclerosis—a post-mortem study of the spinal cord. *J Neurol*. 2003; 250(11):1293–301. <https://doi.org/10.1007/s00415-003-0192-3>
  53. Lazari A, Lipp I. Can MRI measure myelin? Systematic review, qualitative assessment, and meta-analysis of studies validating microstructural imaging with myelin histology. *Neuroimage*. 2021; 230:117744. <https://doi.org/10.1016/j.neuroimage.2021.117744>
  54. Reeves C, Tachrount M, Thomas D, Michalak Z, Liu J, Ellis M, et al. Combined ex vivo 9.4T MRI and quantitative histopathological study in Normal and pathological neocortical resections in focal epilepsy. *Brain Pathol*. 2016;26(3):319–33. <https://doi.org/10.1111/bpa.12298>
  55. Tardif CL, Bedell BJ, Eskildsen SF, Collins DL, Pike GB. Quantitative magnetic resonance imaging of cortical multiple sclerosis pathology. *Mult Scler Int*. 2012;2012:e742018. <https://doi.org/10.1155/2012/742018>
  56. Laule C, Kozlowski P, Leung E, Li DKB, Mackay AL, Moore GRW. Myelin water imaging of multiple sclerosis at 7 T: correlations with histopathology. *Neuroimage*. 2008;40(4):1575–80. <https://doi.org/10.1016/j.neuroimage.2007.12.008>
  57. Schmierer K, Wheeler-Kingshott CAM, Boulby PA, Scaravilli F, Altmann DR, Barker GJ, et al. Diffusion tensor imaging of post mortem multiple sclerosis brain. *Neuroimage*. 2007;35(2):467–77. <https://doi.org/10.1016/j.neuroimage.2006.12.010>
  58. Preziosa P, Kiljan S, Steenwijk MD, Meani A, van de Berg WDJ, Schenk GJ, et al. Axonal degeneration as substrate of fractional anisotropy abnormalities in multiple sclerosis cortex. *Brain*. 2019; 142(7):1921–37. <https://doi.org/10.1093/brain/awz143>
  59. Ponath G, Park C, Pitt D. The role of astrocytes in multiple sclerosis. *Front Immunol*. 2018;9:217. <https://doi.org/10.3389/fimmu.2018.00217>
  60. Absinta M, Maric D, Gharagozloo M, Garton T, Smith MD, Jin J, et al. A lymphocyte–microglia–astrocyte axis in chronic active multiple sclerosis. *Nature*. 2021;597(7878):709–14. <https://doi.org/10.1038/s41586-021-03892-7>
  61. Popescu BF, Frischer JM, Webb SM, Tham M, Adiele RC, Robinson CA, et al. Pathogenic implications of distinct patterns of iron and zinc in chronic MS lesions. *Acta Neuropathol (Berl)*. 2017;134(1):45–64. <https://doi.org/10.1007/s00401-017-1696-8>
  62. Luchicchi A, Hart B, Frigerio I, et al. Axon-myelin unit blistering as early event in MS Normal appearing white matter. *Ann Neurol*. 2021;89(4):711–25. <https://doi.org/10.1002/ana.26014>

## SUPPORTING INFORMATION

Additional supporting information can be found online in the Supporting Information section at the end of this article.

**How to cite this article:** Galbusera R, Bahn E, Weigel M, Schaedelin S, Franz J, Lu P-J, et al. Postmortem quantitative MRI disentangles histological lesion types in multiple sclerosis. *Brain Pathology*. 2022. e13136. <https://doi.org/10.1111/bpa.13136>